

Orbital Fluctuation Mediated Superconductivity in Iron Pnictides: Analysis of Five Orbital Hubbard-Holstein Model

Hiroshi KONTANI¹, and Seiichiro ONARI²

¹ *Department of Physics, Nagoya University and JST, TRIP, Furo-cho, Nagoya 464-8602, Japan.*

² *Department of Applied Physics, Nagoya University and JST, TRIP, Furo-cho, Nagoya 464-8602, Japan.*

(Dated: February 4, 2022)

In iron pnictides, we find that the moderate electron-phonon interaction due to the Fe-ion oscillation can induce the critical d -orbital fluctuations, without being prohibited by the Coulomb interaction. These fluctuations give rise to the strong pairing interaction for the s -wave superconducting (SC) state without sign reversal (s_{++} -wave state), which is consistent with experimentally observed robustness of superconductivity against impurities. When the magnetic fluctuations due to Coulomb interaction are also strong, the SC state shows a smooth crossover from the s -wave state with sign reversal (s_{\pm} -wave state) to the s_{++} -wave state as impurity concentration increases.

PACS numbers: 74.70.Xa, 74.20.-z, 74.20.Rp

The mechanism of high- T_c superconductivity in iron pnictides has been an important open problem. By considering the Coulomb interaction at Fe-ions, antiferromagnetic (AFM) fluctuation mediated fully-gapped sign-reversing s -wave state (s_{\pm} -wave state) is expected theoretically [1, 2]. Regardless of the beauty of the mechanism, there are several serious discrepancies for the s_{\pm} -wave state. For example, although s_{\pm} -wave state is expected to be very fragile against impurities due to the interband scattering [3], the superconducting (SC) state is remarkably robust against impurities [4] and α -particle irradiation [5]. Moreover, clear “resonance-like” peak structure observed by neutron scattering measurements [6] is reproduced by considering the strong correlation effect via quasiparticle damping, without the necessity of sign reversal in the SC gap [7]. These facts indicate that a conventional s -wave state without sign reversal (s_{++} -wave state) is also a possible candidate for iron pnictides.

Then, a natural question is whether the electron-phonon (e -ph) interaction is important or not. Although first principle study predicts small e -ph coupling constant $\lambda \sim 0.21$ [8], several experiments indicate the significance of e -ph interaction. For example, the structural transition temperature T_S is higher than the Neel temperature in underdoped compounds, although the structural distortion is small. Also, prominent softening of shear modulus is observed towards T_S or T_c in Ba122 [9]. Raman spectroscopy [10] also indicates larger e -ph interaction.

Interestingly, there are several “high- T_c ” compounds with nodal SC gap structure, like $\text{BaFe}_2(\text{As}_{1-x}\text{P}_x)_2$ [11] and some 122 systems [12]. Although nodal s_{\pm} -wave state can appear in the spin-fluctuation scenario due to the competition between the dominant $\mathbf{Q} = (\pi, 0)$ and subdominant fluctuations [1, 13], the T_c is predicted to be very low. Thus, it is a crucial challenge to explain the rich variety of the gap structure in high- T_c compounds.

In this letter, we introduce the five-orbital Hubbard-Holstein (HH) model for iron pnictides, considering the e -ph interaction by Fe-ion vibrations. We reveal that a

relatively small e -ph interaction ($\lambda \lesssim 0.3$) induces the large orbital fluctuations, which can realize the high- T_c s_{++} -wave SC state. Moreover, the orbital fluctuations are *accelerated* by Coulomb interaction. In the presence of impurities, the s_{++} -wave state dominates the s_{\pm} -wave state for wide range of parameters.

First, we derive the e -ph interaction term, considering only Einstein-type Fe-ion oscillations for simplicity. Here, we describe the d -orbitals in the XYZ -coordinate [1], which is rotated by $\pi/4$ from the xyz -coordinate given by the Fe-site square lattice: We write Z^2 , XZ , YZ , X^2-Y^2 , and XY orbitals as 1, 2, 3, 4, and 5, respectively [1]. We calculate the e -ph matrix elements due to the Coulomb potential, by following Ref. [14]. The potential for a d -electron at \mathbf{r} (with the origin at the center of Fe-ion) due to the surrounding As^{3-} -ion tetrahedron is $U^{\pm}(\mathbf{r}; \mathbf{u}) = 3e^2 \sum_{s=1}^4 |\mathbf{r} + \mathbf{u} - \mathbf{R}_s^{\pm}|^{-1}$, where \mathbf{u} is the displacement vector of the Fe-ion, and \mathbf{R}_s^{\pm} is the location of surrounding As-ions; $\sqrt{3}\mathbf{R}_s^{+}/R_{\text{Fe-As}} = (\pm\sqrt{2}, 0, 1)$ and $(0, \pm\sqrt{2}, -1)$ for $\text{Fe}^{(1)}$, and $\sqrt{3}\mathbf{R}_s^{-}/R_{\text{Fe-As}} = (\pm\sqrt{2}, 0, -1)$ and $(0, \pm\sqrt{2}, 1)$ for $\text{Fe}^{(2)}$ in the unit cell with two Fe-sites. Note that $u_{X,Y}$ and u_Z belong to E_g and B_{1g} phonons [10]. The \mathbf{u} linear term of U^{\pm} , which gives the e -ph interaction, is obtained as $V^{\pm}(\mathbf{r}; \mathbf{u}) = \pm A[2XZ \cdot u_X - 2YZ \cdot u_Y + (X^2 - Y^2)u_Z] + O(r^4)$, where $A = 30e^2/\sqrt{3}R_{\text{Fe-As}}^4$. Then, its nonzero matrix elements are given as

$$\begin{aligned} \langle 2|V|4 \rangle &= \pm 2a^2 A u_X / 7, & \langle 3|V|4 \rangle &= \pm 2a^2 A u_Y / 7, \\ \langle 2|V|2 \rangle &= \pm 2a^2 A u_Z / 7, & \langle 3|V|3 \rangle &= \mp 2a^2 A u_Z / 7, \end{aligned} \quad (1)$$

where a is the radius of d -orbital. Here, we consider $\langle i|V|j \rangle$ only for orbitals $i, j = 2 \sim 4$ that compose the Fermi surfaces (FSs) in Fig. 1 (a) [1]. The obtained e -ph interaction does not couple to the charge density since $\langle i|V|j \rangle$ is trace-less. Thus, the Thomas-Fermi screening for the coefficient A is absent. The local phonon Green function is $D(\omega_l) = 2\bar{u}_0^2 \omega_D / (\omega_l^2 + \omega_D^2)$, which is given by the Fourier transformation of $\langle T_{\tau} u_{\mu}(\tau) u_{\mu}(0) \rangle$ ($\mu = X, Y, Z$). $\bar{u}_0 = \sqrt{\hbar/2M_{\text{Fe}}\omega_D}$ is the position uncertainty

of Fe-ions, ω_D is the phonon frequency, and $\omega_l = 2\pi lT$ is the boson Matsubara frequency. Then, for both $\text{Fe}^{(1)}$ and $\text{Fe}^{(2)}$, the phonon-mediated interaction is given by

$$\begin{aligned} V_{24,42} = V_{34,43} &= -(2Aa^2/7)^2 D(\omega_l) \equiv -g(\omega_l), \\ V_{22,22} = V_{33,33} &= -V_{22,33} = -g(\omega_l), \end{aligned} \quad (2)$$

as shown in Fig. 1 (b). Note that $V_{ll',mm'}$ is symmetric with respect to $l \leftrightarrow l'$, $m \leftrightarrow m'$, and $(ll') \leftrightarrow (mm')$. We obtain $g(0) \approx 0.4$ eV if we put $R_{\text{Fe-As}} \approx 2.4$ Å, $a \approx 0.77$ Å (Shannon crystal radius of Fe^{2+}), and $\omega_D \approx 0.018$ eV. We have neglected the e -ph coupling due to d - p hybridization [14] considering the modest d - p hybridization in iron pnictides [15]. Thus, we obtain the multi-orbital HH model for iron pnictides by combining eq. (2) with the on-site Coulomb interaction; the intra- (inter-) orbital Coulomb U (U'), Hund coupling J , and pair-hopping J' .

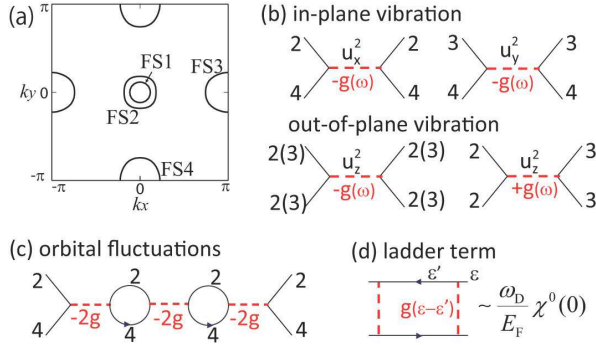


FIG. 1: (Color online) (a) FSs in the unfolded Brillouin zone. (b) Phonon-mediated electron-electron interaction. (c) A bubble-type diagram that induces the critical orbital fluctuations between (2,4) orbitals. (d) A ladder-type diagram that is ignorable when $\omega_D \ll E_F$.

Now, we study the rich electronic properties realized in the multi-orbital HH model [16]. The irreducible susceptibility in the five-orbital model is given by $\chi_{ll',mm'}^0(q) = -(T/N) \sum_k G_{lm}^0(k+q) G_{m'l'}^0(k)$, where $\hat{G}^0(k) = [i\epsilon_n + \mu - \hat{H}_k^0]^{-1}$ is the d -electron Green function in the orbital basis: $q = (\mathbf{q}, \omega_l)$, $k = (\mathbf{k}, \epsilon_n)$, and $\epsilon_n = (2n+1)\pi T$ is the fermion Matsubara frequency. μ is the chemical potential, and \hat{H}_k^0 is the kinetic term given in Ref. [1]. Then, the susceptibilities for spin and charge sectors in the random-phase-approximation (RPA) are given as [17]

$$\hat{\chi}^{s(c)}(q) = \hat{\chi}^0(q) [1 - \hat{\Gamma}^{s(c)} \hat{\chi}^0(q)]^{-1}. \quad (3)$$

For the spin channel, $\Gamma_{l_1 l_2, l_3 l_4}^s = U, U', J$, and J' for $l_1 = l_2 = l_3 = l_4$, $l_1 = l_3 \neq l_2 = l_4$, $l_1 = l_2 \neq l_3 = l_4$, and $l_1 = l_4 \neq l_2 = l_3$, respectively [1]. For the charge channel, $\hat{\Gamma}^c = -\hat{C} - 2\hat{V}(\omega_l)$, where $\hat{V}(\omega_l)$ is given in eq. (2), and $C_{l_1 l_2, l_3 l_4} = U, -U' + 2J, 2U' - J$, and J' for $l_1 = l_2 = l_3 = l_4$, $l_1 = l_3 \neq l_2 = l_4$, $l_1 = l_2 \neq l_3 = l_4$, and $l_1 = l_4 \neq l_2 = l_3$, respectively [1]. Figure 1 (c)

shows one of bubble diagrams for (2,4)-channel due to the “negative exchange coupling $V_{24,42}$ ” that leads to a critical enhancement of $\hat{\chi}^c(q)$ [18]. We neglect the ladder diagrams given by $\hat{V}(\omega_l)$ in Fig. 1 (d) since $\omega_D \ll W_{\text{band}}$ [8, 10]. We put $\omega_D = 0.02$ eV, $U'/U = 0.69$, $J/U = 0.16$ and $J = J'$, and fix the electron number $n = 6.1$ (10% electron doping); the density of states per spin is $N(0) = 0.66$ [eV $^{-1}$]. Numerical results are not sensitive to these parameters. We use 128^2 \mathbf{k} -meshes, and 512 Matsubara frequencies. Hereafter, the unit of energy is eV.

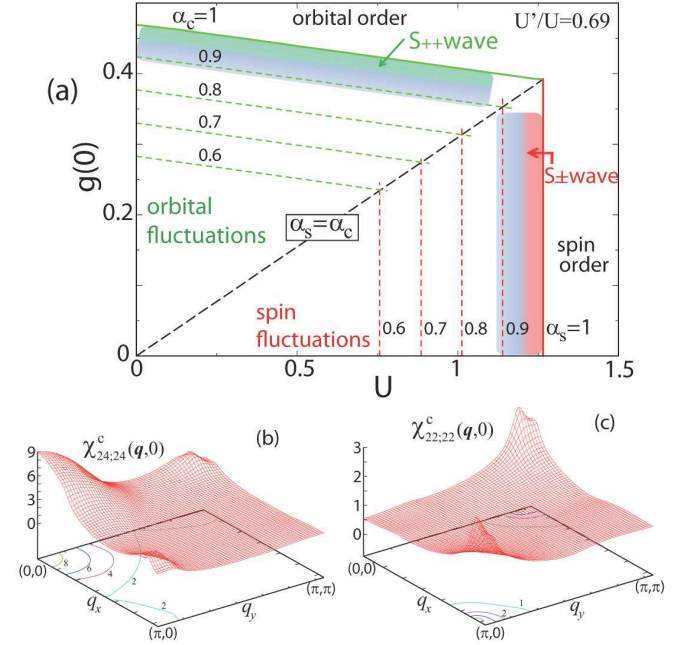


FIG. 2: (Color online) (a) Obtained U - $g(0)$ phase diagram. (b) Obtained $\chi_{24,42}^c(\mathbf{q}, 0)$ and $\chi_{22,22}^c(\mathbf{q}, 0)$ for $\alpha_c = 0.97$.

Figure 2 (a) shows the obtained U - $g(0)$ phase diagram. $\alpha_{s(c)}$ is the spin (charge) Stoner factor, given by the maximum eigenvalue of $\hat{\Gamma}^{s(c)} \hat{\chi}^0(\mathbf{q}, 0)$. Then, the enhancement factor for $\chi^{s(c)}$ is $(1 - \alpha_{s(c)})^{-1}$, and $\alpha_{s(c)} = 1$ gives the spin (orbital) order boundary. Due to the nesting of the FSs, the AFM fluctuation with $\mathbf{Q} \approx (\pi, 0)$ develops as U increases, and s_{\pm} -wave state is realized for $\alpha_s \lesssim 1$ [1]. In contrast, we find that the orbital fluctuations develop as $g(0)$ increases. For $U = 1$, the critical value $g_{\text{cr}}(0)$ for $\alpha_c = 1$ is 0.4, and the critical e -ph coupling constant is $\lambda_{\text{cr}} \equiv g_{\text{cr}}(0)N(0) = 0.26$ [19]. Since the obtained λ_{cr} is close to λ given by the first principle study [8], strong orbital fluctuations are expected to occur in iron pnictides. At fixed U , λ_{cr} decreases as J/U approaches zero.

Figure 2 (b) and (c) show the obtained $\chi_{ll',mm'}^c(\mathbf{q}, 0)$ for $(ll', mm') = (24, 42)$ and $(22, 22)$, respectively, for $U = 1.14$ and $\alpha_c = 0.97$ ($g(0) = 0.40$): Both of them are the most divergent channels for electron-doped cases. The enhancement of (24,42)-channel is induced by the multiple scattering by $V_{24,42}$. The largest broad peak around $\mathbf{q} = (0, 0)$ originates from the forward scat-

tering in the electron-pocket (FS3 or 4) composed of 2 ~ 4 orbitals. (FS1,2 are composed of only 2 and 3 orbitals.) These ferro-orbital fluctuations would induce the softening of shear modulus [9], and also reinforce the ferro-orbital-ordered state below T_S [20] that had been explained by different theoretical approaches [21]: The divergence of $\chi_{24,42}^c$ ($\chi_{34,43}^c$) pushes the 2,4 (3,4) orbitals away from the Fermi level, and the Fermi surfaces in the ordered state will be formed only by 3 (2) orbital, consistently with ref. [20]. The lower peak around $\mathbf{Q} = (\pi, 0)$ comes from the nesting between hole- and electron-pockets. Also, the enhancement of (22, 22)-channel for $\mathbf{Q} = (\pi, 0)$ is induced by the nesting via multiple scattering by $V_{22,22}$ and $V_{22,33}$. In contrast, the charge susceptibility $\sum_{l,m} \chi_{ll,mm}^c(\mathbf{q}, 0)$ is finite even if $\alpha_c \rightarrow 1$ since $\chi_{22,33}^c \approx -\chi_{22,22}^c$.

Now, we will show that large orbital fluctuations, which are not considered in the first principle study of T_c [8], can induce the s_{++} -wave state when $g(0) > 0$. We analyze the following linearized Eliashberg equation using the RPA [1], by taking both the spin and orbital fluctuations into account on the same footing:

$$\lambda_E \Delta_{ll'}(k) = \frac{T}{N} \sum_{k', m_i} W_{lm_1, m_4 l'}(k - k') \times G_{m_1 m_2}(k') \Delta_{m_2 m_3}(k') G_{m_4 m_3}(-k'), \quad (4)$$

where $\hat{W}(q) = -\frac{3}{2} \hat{\Gamma}^s \hat{\chi}^s(q) \hat{\Gamma}^s + \frac{1}{2} \hat{\Gamma}^c \hat{\chi}^c(q) \hat{\Gamma}^c - \frac{1}{2} (\hat{\Gamma}^s - \hat{\Gamma}^c)$ for singlet states. The eigenvalue λ_E increases as $T \rightarrow 0$, and it reaches unity at $T = T_c$. In addition, we take the impurity effect into consideration since many iron pnictides show relatively large residual resistivity. Here, we assume the Fe site substitution, where the impurity potential I is diagonal in the d -orbital basis [3]. Then, the T -matrix in the normal state is given by $\hat{T}(\epsilon_n) = [I^{-1} - N^{-1} \sum_{\mathbf{k}} \hat{G}(\mathbf{k}, \epsilon_n)]^{-1}$ in the orbital basis [3]. Then, the normal self-energy is $\hat{\Sigma}^n(\epsilon_n) = n_{\text{imp}} \hat{T}(\epsilon_n)$, where n_{imp} is the impurity concentration. Also, the linearized anomalous self-energy is given by

$$\Sigma_{ll'}^a(\epsilon_n) = \frac{n_{\text{imp}}}{N} \sum_{\mathbf{k}, m_i} T_{lm_1}(\epsilon_n) G_{m_1 m_2}(\mathbf{k}, \epsilon_n) \Delta_{m_2 m_3}(\mathbf{k}, \epsilon_n) \times G_{m_4 m_3}(-\mathbf{k}, -\epsilon_n) T_{l' m_4}(-\epsilon_n). \quad (5)$$

Then, the Eliashberg equation for $n_{\text{imp}} \neq 0$ is given by using the full Green function $\hat{G}(k) = [i\epsilon_n + \mu - \hat{H}_{\mathbf{k}}^0 - \hat{\Sigma}^n(\epsilon_n)]^{-1}$ in eqs. (4) and (5), and adding $\Sigma_{ll'}^a(\epsilon_n)$ to the right hand side of eq. (4). Hereafter, we solve the equation at relatively high temperature $T = 0.02$ since the number of \mathbf{k} -meshes (128^2) is not enough for $T < 0.02$, due to the fact that k_F in iron pnictides is only $1/5$ of that in cuprate superconductors.

Figure 3 shows the n_{imp} -dependence of λ_E at $\alpha_c = 0.98$, for $U = 1.11, 1.14$ and 1.18 . Considering large $\lambda_E \gtrsim 0.8$ at $T = 0.02$, relatively high- T_c ($\lesssim 0.02$) is expected. For the smallest U ($U = 1.11$; $\alpha_s = 0.85$), we find that

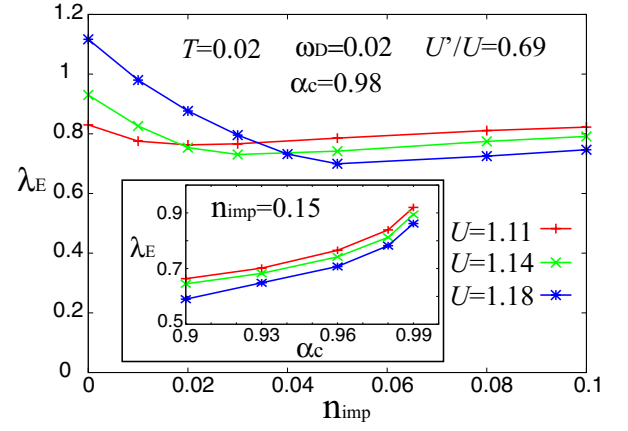


FIG. 3: (Color online) n_{imp} -dependence of λ_E at $\alpha_c = 0.98$. If we put $g(0) = 0$ (s_{\pm} -state), λ_E at $n_{\text{imp}} = 0$ decreases by $0.1 \sim 0.15$, since the ferro-orbital fluctuations enhance both s_{++} and s_{\pm} wave states. Inset: α_c -dependence of λ_E .

nearly isotropic s_{++} -wave state is realized; the obtained λ_E is almost independent of n_{imp} , indicating the absence of impurity effect on the s_{++} -wave state, as discussed in Refs. [3, 22]. For the largest U ($U = 1.18$; $\alpha_s = 0.91$), s_{\pm} -wave state is realized at $n_{\text{imp}} = 0$; λ_E decreases slowly as n_{imp} increases from zero, whereas it saturates for $n_{\text{imp}} \geq 0.05$, indicating the smooth crossover from s_{\pm} - to s_{++} -wave states due to the interband impurity scattering. For $U = 1.14$ ($\alpha_s = 0.88$), the SC gap at $n_{\text{imp}} = 0$ is a hybrid of s_{++} and s_{\pm} ; only Δ_{FS2} is different in sign.

The inset of Fig. 3 shows λ_E for s_{++} -wave state in the presence of impurities ($n_{\text{imp}} = 0.15$): Since $\lambda_E(\alpha_c = 0.98) - \lambda_E(\alpha_c = 0.90)$ is only ~ 0.15 for each value of U , we expect that relatively large T_c for s_{++} -wave state is realized even if orbital fluctuations are moderate. We stress that the obtained λ_E is almost constant for $\omega_D = 0.02 \sim 0.1$, suggesting the absence of isotope effect in the s_{++} -wave state due to the strong retardation effect [14]. By the same reason, λ_E for the s_{++} -wave state is seldom changed if we put $U = 3$ in the Hartree-Fock term $\frac{1}{2}(\hat{\Gamma}^s - \hat{\Gamma}^c)$ in $W(q)$, indicating that the Morel-Anderson pseudo-potential almost saturates.

Here, we discuss the case $U = 1.18$ in detail: Figure 4 shows the SC gap on the FSs in the band-representation for (a) $n_{\text{imp}} = 0$, (b) 0.03, and (c) 0.08. They satisfy the condition $N^{-1} \sum_{\mathbf{k}, lm} |\Delta_{lm}(\mathbf{k})|^2 = 1$. The horizontal axis is the azimuth angle for the \mathbf{k} -point with the origin at Γ (M) point for FS1,2 (FS4); $\theta = 0$ corresponds to the k_x -direction. In case (a), s_{\pm} -state with strong imbalance, $|\Delta_{\text{FS1}}|, |\Delta_{\text{FS2}}| \ll \Delta_{\text{FS4}}$, is realized, and Δ_{FS4} takes the largest value at $\theta = \pi/2$, where the FS is mainly composed of orbital 4. In case (c), impurity-induced isotropic s_{++} -state [23] with $\Delta_{\text{FS1}} \sim \Delta_{\text{FS2}} \sim \Delta_{\text{FS4}}$ is realized, consistently with many ARPES measurements [24]. In case (b), $\Delta_{\mathbf{k}}$ on FS1 is almost gapless. However, considering the k_z -dependence of the FSs, a (horizontal-

type) nodal structure is expected to appear on FS1,2. In real compounds with $T_c \sim 50\text{K}$, the $s_{\pm} \rightarrow s_{++}$ crossover should be induced by small residual resistivity $\rho_{\text{imp}} \sim 20 \mu\Omega\text{cm}$ ($n_{\text{imp}} \sim 0.01$ for $I = 1$), as estimated in Ref. [3].

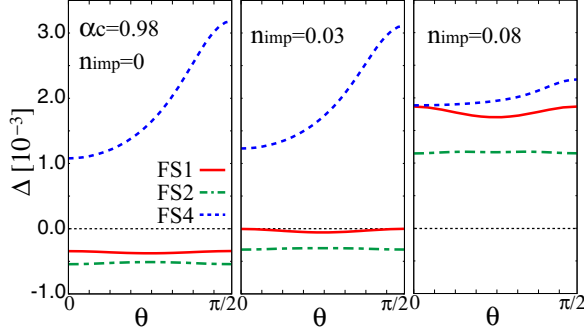


FIG. 4: (Color online) SC gap functions for $U = 1.18$ as functions of θ at (a) $n_{\text{imp}} = 0$, (b) 0.03, and (c) 0.08, respectively.

We comment that at $n_{\text{imp}} = 0$, s_{\pm} -wave state is realized in the RPA even if $\alpha_s \lesssim \alpha_c$, due to factor 3 in front of $\frac{1}{2}\hat{\Gamma}^s\hat{\chi}^s(q)\hat{\Gamma}^s$ in $W(q)$. For the same reason, however, reduction in α_s (or increment of U_{cr} for $\alpha_s = 1$) due to the “self-energy correction by U ” is larger, which will be unfavorable for the s_{\pm} -wave state. Therefore, self-consistent calculation for the self-energy is required to discuss the value of $\alpha_{c,s}$ and the true pairing state.

Here, we discuss where in the α_s - α_c phase diagram in Fig. 2 (a) real compounds are located. Considering the weak T -dependence of $1/T_1T$ in electron-doped SC compounds [25], we expect that they belong to the area $\alpha_c \gg \alpha_s$. Then, s_{++} -wave SC state will be realized without (or very low density) impurities, like the case of $U = 1.11$ or 1.14 in Fig. 3. On the other hand, impurity-induced $s_{\pm} \rightarrow s_{++}$ crossover may be realized in $\text{BaFe}_2(\text{As}_{1-x}\text{P}_x)_2$ (undoped) or $(\text{Ba}_{1-x}\text{K}_x)\text{Fe}_2\text{As}_2$ (hole-doped) SC compounds, where AFM fluctuations are rather strong.

Finally, we discuss the non-Fermi-liquid-like transport phenomena in iron pnictides. For example, the resistivity is nearly linear-in- T , and the Hall coefficient R_H increases at lower temperatures [4, 26]. Although the forward scattering induced by ferro-orbital fluctuations might be irrelevant, antiferro-orbital and AFM fluctuations with $\mathbf{Q} = (\pi, 0)$ are expected to cause the anomalous transport, due to the current vertex correction [27].

In summary, we have proposed a mechanism of s_{++} -wave SC state induced by orbital fluctuations, due to the phonon-mediated electron-electron interaction. Three orbitals (XZ , YZ and $X^2 - Y^2$) are necessary to leads the ferro-orbital fluctuations. The SC gap structure drastically changes depending on parameters α_s , α_c , and n_{imp} , consistently with observed rich variety of the gap structure that is a salient feature of iron pnictides. Orbital fluctuation mediated s_{++} -wave state is also obtained for

hole-doped cases, although the antiferro-orbital fluctuations becomes stronger than the ferro-orbital ones.

The s -wave superconductivity induced by orbital fluctuations had been discussed in Ref. [17] for $U' > U$; this condition can be realized by including the A_{1g} -phonon [28]. In the present model, however, A_{1g} -phonon is negligible since $g_{\text{cr}}(0)$ given by A_{1g} -phonon is much greater than $g_{\text{cr}}(0) \sim 0.4$ in Fig. 2 (a): The ferro-orbital fluctuations in Fig. 2 (b) originate from the *negative* exchange interaction caused by E_g -phonon, as shown in Fig. 1 (c).

We thank D.S. Hirashima, M. Sato, Y. Matsuda, Y. Ōno and Y. Yanagi for valuable discussions. This study has been supported by Grants-in-Aid for Scientific Research from MEXT of Japan, and by JST, TRIP.

Note added in proof: After the acceptance of this work, we found that $g_{\text{cr}}(0) \sim 0.4$ in Fig. 2 (a) is reduced to half if all the e -ph matrix elements including 1, 5 orbitals are taken into account. Results similar to Fig. 3 are obtained by using $g(0) \sim 0.2$, whereas (vertical-type) nodes appear on FS3,4 during the $s_{++} \rightarrow s_{\pm}$ crossover for $U = 1.18$.

-
- [1] K. Kuroki *et al.*, Phys. Rev. Lett. **101**, 087004 (2008).
 - [2] I. I. Mazin *et al.*, Phys. Rev. Lett. **101**, 057003 (2008).
 - [3] S. Onari and H. Kontani, Phys. Rev. Lett. **103** 177001 (2009).
 - [4] A. Kawabata *et al.*, J. Phys. Soc. Jpn. **77** (2008) Suppl. C 103704; M. Sato *et al.*, J. Phys. Soc. Jpn. **79** (2009) 014710; S.C. Lee *et al.*, J. Phys. Soc. Jpn. **79** (2010) 023702.
 - [5] C. Tarantini *et al.*, arXiv:0910.5198.
 - [6] A. D. Christianson, *et al.*, Nature **456**, 930 (2008).
 - [7] S. Onari *et al.*, Phys. Rev. B **81**, 060504(R) (2010).
 - [8] L. Boeri *et al.*, Phys. Rev. Lett. **101**, 026403 (2008).
 - [9] R.M. Fernandes *et al.*, arXiv:0911.3084.
 - [10] M. Rahlenbeck *et al.*, Phys. Rev. B **80**, 064509 (2009).
 - [11] K. Hashimoto *et al.*, arXiv:0907.4399.
 - [12] C. Martin *et al.*, Phys. Rev. B **81**, 060505(R) (2010).
 - [13] T.A. Maier, *et al.*, Phys. Rev. B **79**, 224510 (2009).
 - [14] K. Yada and H. Kontani, Phys. Rev. B **77**, 184521 (2008).
 - [15] D.J. Singh, Physica C **469**, 418 (2009).
 - [16] J.E. Han *et al.*, Phys. Rev. Lett. **90**, 167006 (2003); M. Capone *et al.*, Phys. Rev. Lett. **93**, 047001 (2004).
 - [17] T. Takimoto *et al.*, J. Phys.: Condens. Matter **14**, L369 (2002).
 - [18] The effect of Coulomb interaction on $\chi_{24,42}^{\varepsilon}(\mathbf{q}, 0)$ is not large if $C_{U',U'} + C_{U',U'} = -U' + J + J'$ is small.
 - [19] λ_i for orbital $i = 2 \sim 4$ is $\lambda_i \approx -\sum_{j=2}^4 N_j(0)V_{ij,ij}(0) = N(0)g(0)$, where $N_j(0)$ is the partial DOS. Then, $\lambda \approx N(0)g(0)$ in the band-diagonal basis.
 - [20] T. Shimojima *et al.*, Phys. Rev. Lett. **104**, 057002 (2010).
 - [21] F. Krüger *et al.*, Phys. Rev. B **79**, 054504 (2009); W. Lv *et al.*, Phys. Rev. B **80**, 224506 (2009); C.C. Lee *et al.*, Phys. Rev. Lett. **103**, 267001 (2009).
 - [22] Above T_c , λ_E slightly *increases* with n_{imp} in conventional s -wave superconductors, but never exceeds unity.
 - [23] V. Mishra *et al.*, Phys. Rev. B **79**, 094512 (2009); D. Markowitz *et al.*, Phys. Rev. **131**, 563 (1963).

- [24] D. V. Evtushinsky *et al.*, New J. Phys. **11**, 055069 (2009).
- [25] T. Nakano *et al.*, Phys. Rev. B **81**, 100510(R) (2010); Y. Nakai *et al.*, Phys. Rev. B **81**, 020503(R) (2010).
- [26] S. Kasahara *et al.*, arXiv:0905.4427.
- [27] H. Kontani, Rep. Prog. Phys. **71**, 026501 (2008).
- [28] Y. Yanagi *et al.*, Phys. Rev. B **81**, 054518 (2010).